

Demonstrating the Manufacture of Human CAR-T Cells in an Automated Stirred-Tank Bioreactor

Elena Costariol, Marco C. Rotondi, Arman Amini, Christopher J. Hewitt, Alvin W. Nienow, Thomas R. J. Heathman, and Qasim A. Rafiq*

Chimeric antigen receptor T-cell (CAR-T) therapies have proven clinical efficacy for the treatment of hematological malignancies. However, CAR-T cell therapies are prohibitively expensive to manufacture. The authors demonstrate the manufacture of human CAR-T cells from multiple donors in an automated stirred-tank bioreactor. The authors successfully produced functional human CAR-T cells from multiple donors under dynamic conditions in a stirred-tank bioreactor, resulting in overall cell yields which were significantly better than in static T-flask culture. At agitation speeds of 200 rpm and greater (up to 500 rpm), the CAR-T cells are able to proliferate effectively, reaching viable cell densities of $>5 \times 10^6$ cells ml⁻¹ over 7 days. This is comparable with current expansion systems and significantly better than static expansion platforms (T-flasks and gas-permeable culture bags). Importantly, engineered T-cells post-expansion retained expression of the CAR gene and retained their cytolytic function even when grown at the highest agitation intensity. This proves that power inputs used in this study do not affect cell efficacy to target and kill the leukemia cells. This is the first demonstration of human CAR-T cell manufacture in stirred-tank bioreactors and the findings present significant implications and opportunities for larger-scale allogeneic CAR-T production.

1. Introduction

Engineered, gene-modified cell therapies have emerged as a promising therapeutic modality for hematological malignancies. Chimeric antigen receptor (CAR) T-cell therapies in particular have demonstrated significant clinical efficacy for conditions such as acute lymphoblastic leukemia and non-Hodgkin's lymphoma and have received US Food and Drug Administration (FDA) and European Medicines Agency (EMA) regulatory approval (e.g., Novartis' Kymriah and Gilead's Yescarta).^[1] Despite the positive clinical outcomes, these patient-specific therapies are expensive to manufacture, cost in excess of \$250 000 and their current manufacture involves open, manual processes.^[2] To reduce the cost, there is a need to improve CAR-T manufacture and develop reproducible production processes that minimize the need for human operator intervention and manual operations.

For patient-specific therapies, such as the current wave of autologous CAR-T products, the approach to scale requires a high-throughput parallel production of multiple, individual product batches. Economies of scale cannot be achieved through a traditional "scale-up approach," rather must focus developing an efficient and effective "scale-out" approach, which will necessitate automated, robust, and closed expansion technologies to ensure individual patient production and effective product segregation. However, given the recent advances in gene-editing tools such as CRISPR-Cas9, zinc finger nuclease, and transcription activator-like effector nuclease, there is increasing focus on developing an off-the-shelf allogeneic CAR-T therapy which would require bulk production and where economies of scale are achieved via a traditional scale-up approach. This necessitates large-scale cell expansion technologies, which can manufacture multiple cell doses per batch and the use of bioreactor technologies with automated process control capability.^[3]


When selecting a suitable expansion platform for cell production, it is important to consider multiple factors to mitigate clinical and commercial risk. The propensity among clinical programs has been to employ easy-to-use platforms such as T-flasks, G-rax bioreactors, and static culture bags. However, it is widely recognized that such systems have poor monitoring and control capability and are limited with respect to scalability.^[2,4] All-in-one

E. Costariol, Dr. M. C. Rotondi, A. Amini, Dr. Q. A. Rafiq
Advanced Centre for Biochemical Engineering, Department of
Biochemical Engineering
University College London
London WC1E 6BT, UK
E-mail: q.rafiq@ucl.ac.uk

Prof. C. J. Hewitt, Prof. A. W. Nienow
Aston Medical Research Institute, School of Life and Health Sciences
Aston University
Birmingham B4 7ET, UK

Prof. A. W. Nienow
School of Chemical Engineering
University of Birmingham
Edgbaston Birmingham B15 2TT, UK

Dr. T. R. J. Heathman
Hitachi Chemical Advanced Therapeutic Solutions (HCATS)
4 Pearl Court Allendale, NJ 07401, USA

 The ORCID identification number(s) for the author(s) of this article can be found under <https://doi.org/10.1002/biot.202000177>

© 2020 The Authors. *Biotechnology Journal* published by WILEY-VCH Verlag GmbH & Co. KGaA, Weinheim. This is an open access article under the terms of the Creative Commons Attribution License, which permits use, distribution and reproduction in any medium, provided the original work is properly cited.

DOI: 10.1002/biot.202000177

systems such as the CliniMACS Prodigy allow multiple process steps to be combined, thereby simplifying the user interactions. However, such systems can currently only be employed as part of a scale-out strategy rather than scale-up due to the limited size of the culture vessel.

The other key platforms under consideration, or currently employed in clinical programs, include hollow-fiber bioreactors and rocking-motion bioreactors. Such systems allow for increased scale (up to 2000 L) with process monitoring and control capability, and can accommodate different modes of operation, for example, fed-batch and perfusion.

If these platforms are compared to stirred-tank bioreactors (STRs), the latter clearly have significant potential advantages. First, they already provide a robust cell expansion platform for both autologous and allogeneic applications, with scales varying from 100 mL through to >20 000 L for large-scale recombinant protein production using Chinese hamster ovary (CHO) cells and other mammalian cell types.^[5] Second, such systems are widely used in the biologics industry, have been characterized extensively for cell production and a proven track record for large-scale industrial manufacture, including recently, single-use STRs up to 2000 L.^[6] They have also now become extensively used at scale for human mesenchymal stem cell culture on microcarriers.^[7] This usage increases the likelihood of adoption for therapeutic development companies who have these manufacturing platforms in place and reduces the risk associated with using such platforms for commercial manufacture. Third, STRs have the added advantage that, unlike rocking-motion bioreactors, they have well characterized and proven high-throughput small-scale models, such as the ambr 15, the ambr 250, and DASbox system among others, that allow working volumes as low as 15–250 mL.^[8,9] These high-throughput systems allow multiple bioreactors to be run in parallel, increase experimental data generation, and provide a well-established bioprocessing pathway to increase in scale from the mL to the multi-liter scale, thereby increasing process understanding and reducing development timeframes. Fourth, STRs have a well-established supply chain infrastructure through their current application in the biopharma industry, significantly reducing supply risk at scale, which is a constraint for the current alternative technologies that often rely on single source suppliers and low product manufacturing volumes. Finally, STRs have an existing and well established pathway to enable full process integration with upstream and downstream unit operations to allow for successful interlinking and automation of multiple process unit operations, which will dramatically reduce the current costs of manufacturing associated with direct labor.

In light of the significant advantages STRs offer over expansion systems, the key uncertainty with their use for such applications is whether they can produce T-cell therapies at the required quality and specification to enable therapeutically effective products. If this can be successfully demonstrated, then therapies above a single-patient dose would be wise to employ an STR. This paper attempts to address this research question.

We previously reported the successful expansion of human primary T-cells in automated STRs (ambr 250) at the 250 mL scale in which it was shown that in spite of unsubstantiated

concerns related to hydrodynamic stress, human primary T-cells could be cultured in STRs and higher cell yields in comparison to static T-flask controls while retaining the key cell quality attributes.^[10] Contrary to the prevailing concerns about the growth of primary T-cells under agitated conditions in a STR, not only did the T-cells grow better than the equivalent static T-flask control, but higher cell yields were obtained with increasing agitation speeds. The study also showed that the magnetic Dynabeads failed to activate the cells in spinner flasks because they attached to the magnetic stir bar; similarly at a very low impeller speed and specific power in the bioreactor, the beads were not suspended but the cells were. Successful culture was achieved at higher speeds and specific powers in two different bioreactors, one baffled with two impellers and one unbaffled with a single larger impeller. It was also shown that when the specific power profile in the two bioreactors matched, the culture performances were essentially identical. Under conditions of adequate Dynabeads suspension, the culture was improved compared to T-flasks with respect to viable cell density and cell quality was maintained.

While the previous study demonstrated the potential for improved human primary T-cell growth in STRs, from a clinical perspective, it is necessary to determine whether genetically-engineered CAR-T cells can be grown in such systems and whether the CAR-T cells retain expression of the CAR and their functional ability to target and kill cancerous cells. In this study, we investigate, for the first time, the expansion of CAR-T cells from multiple donors in automated STRs with respect to their cell growth kinetics and quality attributes, and investigate whether the phenomenon of increasing cell density with increasing agitation speeds (and increasing specific powers) continues at even higher speeds (up to 500 rpm, $1164 \times 10^{-4} \text{ W kg}^{-1}$) than investigated in the original study which only went up to 200 rpm ($74 \times 10^{-4} \text{ W kg}^{-1}$).

2. Results

2.1. CAR-T Cell Growth Kinetics under Different Agitation Conditions

As described above, the growth kinetics and quality profile of engineered CAR-T cells was investigated, for the first time, in a STR. The unbaffled ambr 250 bioreactor was used and operated at agitation speeds of 100, 200, 300, 400, and 500 rpm. CAR-T cells were grown in T-flasks as a static control. The feeding regime was kept the same for all the conditions and the viability and live cell concentration was assessed daily as were the growth, metabolite flux, pH, and dO_2 over the 7 days of culture (Figures 1–4).

Although the difference was not found to be statistically significant ($p > 0.05$), higher final cell densities were achieved under the agitated STR conditions (particularly at speeds ≥ 200 rpm) compared to the static T-flask control (Figure 1A,B). This result aligns with what was found previously with primary non-transduced T-cells,^[10] reinforcing the findings of the previous study with primary T-cells.^[10] Clearly, T-cells are able to not only withstand the hydrodynamic forces in a STR, but have greater proliferative capacity compared to static culture conditions.

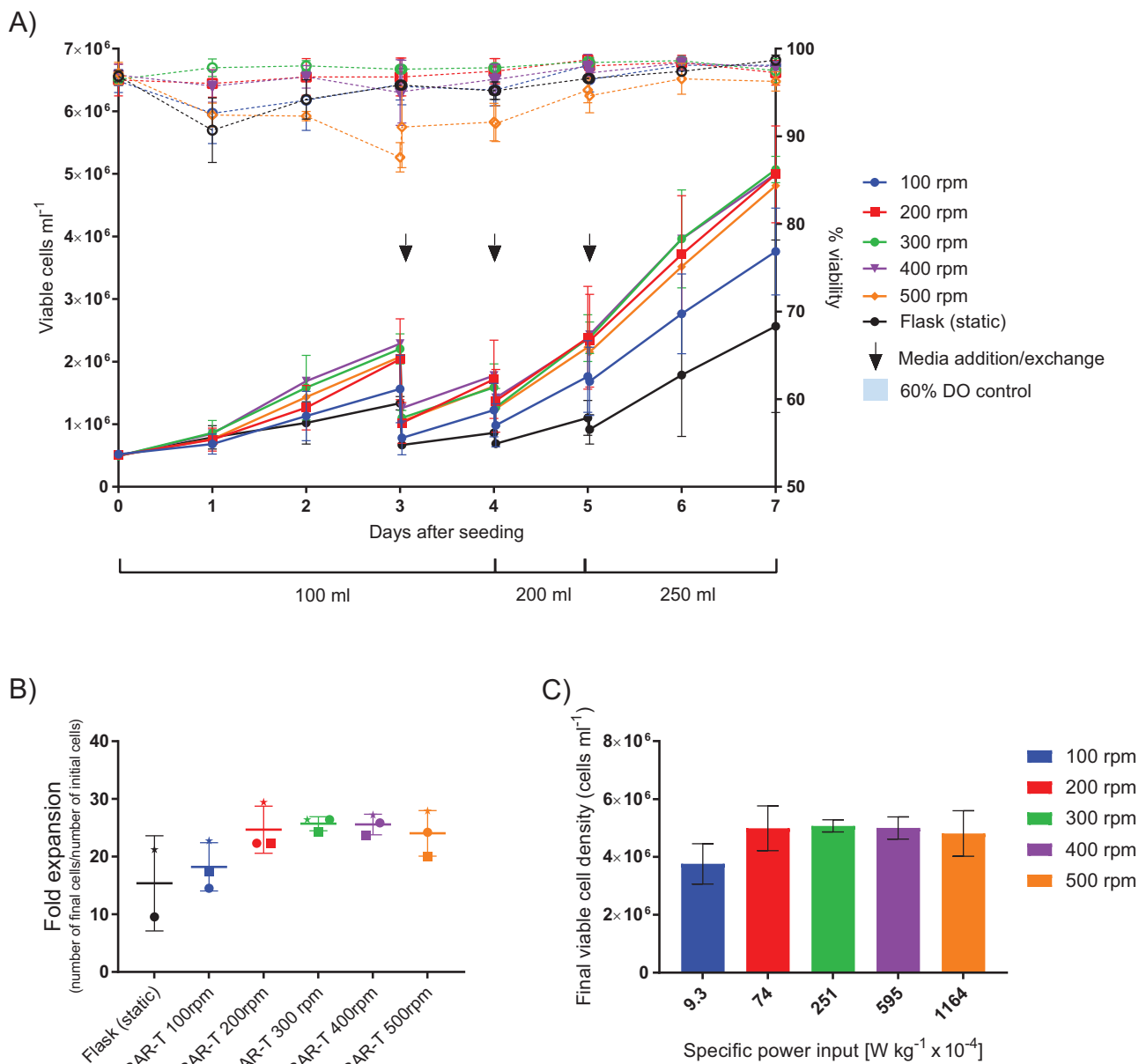


Figure 1. The growth of CAR-T cells from three donors over 7 days in the unbaffled ambr 250 STR at different agitation speeds ($n = 3$). The black arrow indicates the medium addition on day 3 (100 mL), day 4 (50 mL), and a medium exchange (100 mL) on day 5. Data shown mean \pm SD of results with all 3 donors. Only 2 donors were used for the static control (HD12, HD16). A) Viable cell density (cells mL^{-1}) and % viability. B) Fold expansion (total number of viable cells on day 7/total number of viable cells at seeding). Each symbol represents one donor (star = HD12; circle = HD16; square = HD18). Data shown mean \pm SD. C) Final viable cell density (cells mL^{-1}) at day 7 plotted against the specific power input ($\text{W kg}^{-1} \times 10^{-4}$) at the end of each run. Data is shown mean \pm SD of results with all 3 donors. No significant difference ($p > 0.05$) was found between the conditions analyzed with a one-way ANOVA test.

At the lowest speed (100 rpm, $9.3 \times 10^{-4} \text{ W kg}^{-1}$), a final cell density of $3.76 \pm 0.69 \times 10^6$ viable cells mL^{-1} (Figure 1A) was obtained, resulting in the lowest fold expansion (18.22 ± 0.42) among the agitation conditions investigated in the ambr 250 bioreactor (Figure 1B). There was an improvement in the cell growth when the agitation speed was increased to 200 rpm ($74 \times 10^{-4} \text{ W kg}^{-1}$), as was found in the previous study with pri-

mary T-cells,^[10] with a final cell density of $4.99 \pm 0.77 \times 10^6$ viable cells mL^{-1} and a fold increase of 24.67 ± 4.10 .

The cell growth kinetics for the 200, 300, 400, and 500 rpm agitation speeds were very similar, with the highest level of growth obtained at 300 rpm, which resulted in a final cell density of $5.07 \pm 0.21 \times 10^6$ viable cells mL^{-1} and a fold expansion at the harvest point of 25.70 ± 1.21 . There was no

statistically significant difference in CAR-T cell yield at day 7 at any of the higher speeds of 200, 300, 400, or 500 rpm (Figure 1C) even though the final specific power input (P/M) over the last three days at the different speeds increased from 74×10^{-4} to $1164 \times 10^{-4} \text{ W kg}^{-1}$. Although speeds higher than 200 rpm did not lead to higher levels of cell proliferation, likely due to nutrient limitations in the medium (discussed later), the viability of CAR-T cells at harvest was greater than 90% for all speeds, suggesting that the cells were not adversely impacted by the higher agitation rates and the associated fluid dynamic stresses. It is worth noting that the highest P/M is higher than that typically used in free suspension culture such as CHO cells.^[5]

2.2. Metabolite Concentrations

The levels of glucose, lactate, glutamine, and ammonia in the medium were measured off-line on a daily basis (Figure 2A–D). For the runs at speeds of 200 rpm and above which exhibited similar growth kinetics, the metabolites measured in the medium follow a similar trend. In each case, the medium was depleted of glucose and glutamine by day 3, which is the likely cause of the reduced growth rate at this time point and the concomitant increase in pH (Figure 3, right hand side). The glucose and glutamine concentrations were consistently depleted throughout the course of the culture despite the regular medium exchanges/additions (indicated by arrows on Figure 2A–D); by day 6, the glucose and glutamine concentrations reach close to 0 mmol L^{-1} , at which point the pH starts to plateau and then slowly increases (Figure 3, right hand side).

With respect to specific metabolite consumption and production rates (Figure 2E–I), it is noted that the 100 rpm agitation intensity results in slightly higher values compared to the other agitation conditions. However, this trend is to be expected given that this is a per cell metric and in the other conditions, there is an increase in the overall cell density resulting in a lower per cell metabolite consumption or production rate given the starting concentration of metabolites is the same in all the conditions. The yield of lactate from glucose, presented in Figure 2G, shows no significant difference between the five agitation rates, with the mean values all below 2 mol^{-1} , the maximum theoretical yield of lactate from glucose. The specific glutamine consumption rate (Figure 2H) shows a similar trend to glucose, the specific consumption lowers as the speed increases. Once again, this lowering is due to an increased number of cells in the 200–500 rpm conditions and a limited amount of glutamine in the medium. Specific ammonia production (Figure 2I) does not show any significant difference among the tested conditions.

2.3. pH and Dissolved Oxygen Concentration

The pH and dO_2 were monitored throughout the duration of 7 days CAR-T expansion with the ambr bioreactor controller software (Figure 3). The spikes observed in the dO_2 profiles are due to the opening of the cap of the bioreactor to allow medium additions and exchange. For all runs, a dO_2 control by gas blending at 60% was started on day 5 after a 100 mL medium exchange. The

dO_2 control is active only when the monitored dO_2 drops below 60%, but does not lower the dO_2 to 60% if the detected value is higher.

The dO_2 (Figure 3, left hand side) was $\approx 85\%$ at inoculation in all the conditions (100–500 rpm). This value fell slightly over the first 3 days at 100 rpm but remained stable during this time at the higher speeds. After medium addition on day 3, a drop in dO_2 occurred, due to an increase in volume (from 100 to 200 mL) and due to an increased cell concentration at the lowest speed (100 rpm) condition in which the k_1a was lowest and could not meet the oxygen demand of the CAR-T cells. At 200 rpm and above, since the cell density and hence the oxygen uptake rate was approximately the same for these agitation speeds, the drop in dO_2 is less pronounced as the speed is increased. This difference is due to the higher k_1a resulting from the increase in agitation. At day 5, when the dO_2 control at 60% became operational, that value was held at all speeds as indicated by the dO_2 profiles (Figure 3, left hand side).

The pH profiles (Figure 3, right hand side) are essentially the same at each speed, roughly correlating as expected with the viable cell concentration and with the lactate production and accumulation in the medium. The rapid increase in the pH profiles indicates the points at which medium additions or exchanges occurred. In all conditions, there was a slight increase in the pH prior to the medium addition at day 3; this increase may indicate a reduction in cell expansion due to the glucose and glutamine limitations in the medium. The same phenomena can be seen again after day 6, when all the glucose and glutamine in the medium have been consumed. The lowest pH was ≈ 6.4 on day 3 in the runs at 100, 200, 300, and 400 rpm (Figure 3A–D).

2.4. Assessment of Cell Quality and Functionality

The immunophenotypic profile of CAR-T cells was assessed via flow cytometry analysis at the beginning (pre-experiment) and at the end of the expansion in the bioreactor and in the T-flask (Figure 4A–D). The CD4 to CD8 ratio (Figure 4A) was higher, although not significantly ($p > 0.05$), in the static control (3.1 ± 0.7) compared to the ambr 250 at different speeds, where it was closer to the desired 1:1 ratio. The CD8 positive subpopulation of CAR-T cells was further analyzed in terms of naïve, central memory, effector memory, and terminally differentiated T-cells. The amount of naïve and terminally differentiated T-cells was lower than 5% in all samples (data not shown). The central memory subpopulation was higher in the pre-experiment sample (39.6 ± 3.8) compared with the samples post-expansion (Figure 4B). The effector memory percentage increased over the 7 days culture in the ambr 250 bioreactor; however, it was still comparable to the static control (T-175 flask) (Figure 4C). As with the findings with primary human T-cells in the previous study,^[10] the proportion of the cell subpopulation is not affected by agitation and is similar irrespective of culture platform (static T-flask or STR).

The expression of the CAR receptor was assessed by flow cytometry at seeding (day 0) and at the end of the 7 days expansion in the bioreactors and in the static control (Figure 4D). The CAR expression at day 7 was normalized to the expression at day 0

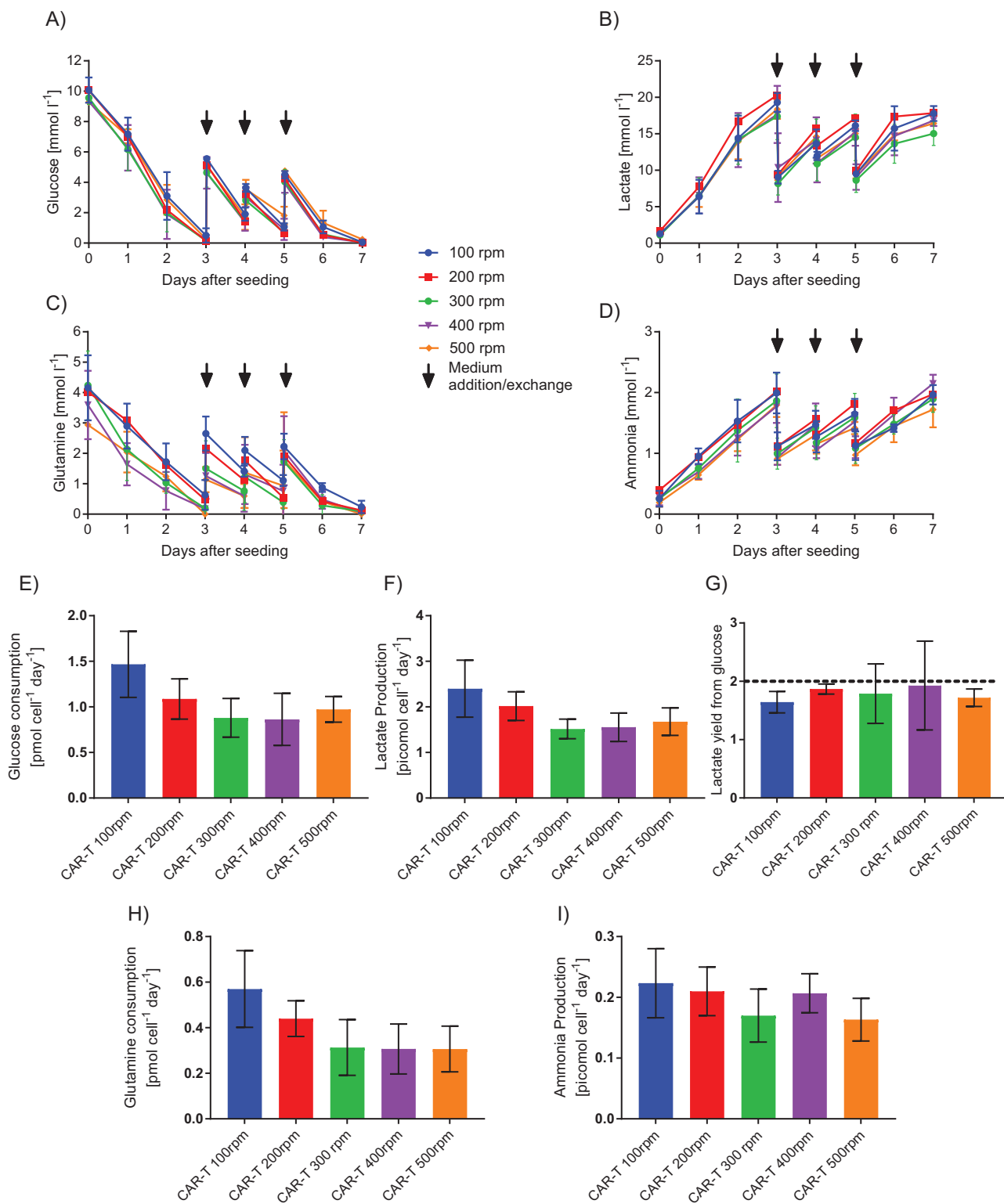


Figure 2. Metabolite concentration [mmol L⁻¹] profiles and specific consumption or production rates [picomol cell⁻¹ day⁻¹] in the ambr 250 unbaffled vessel at different impeller speeds. The black arrows indicate a medium addition/exchange. Data shown as mean ± SD, n = 3. A) Glucose concentration. B) Lactate concentration. C) Glutamine concentration. D) Ammonia concentration. E) Specific glucose consumption rate. F) Specific lactate production rate. G) Yields of lactate from glucose. Reference line at 2 is the maximum theoretical yield of lactate from glucose. H) Specific glutamine consumption rate. I) Specific ammonia production rate. No significant difference (p > 0.05) was found between the conditions analyzed with a one-way ANOVA test.

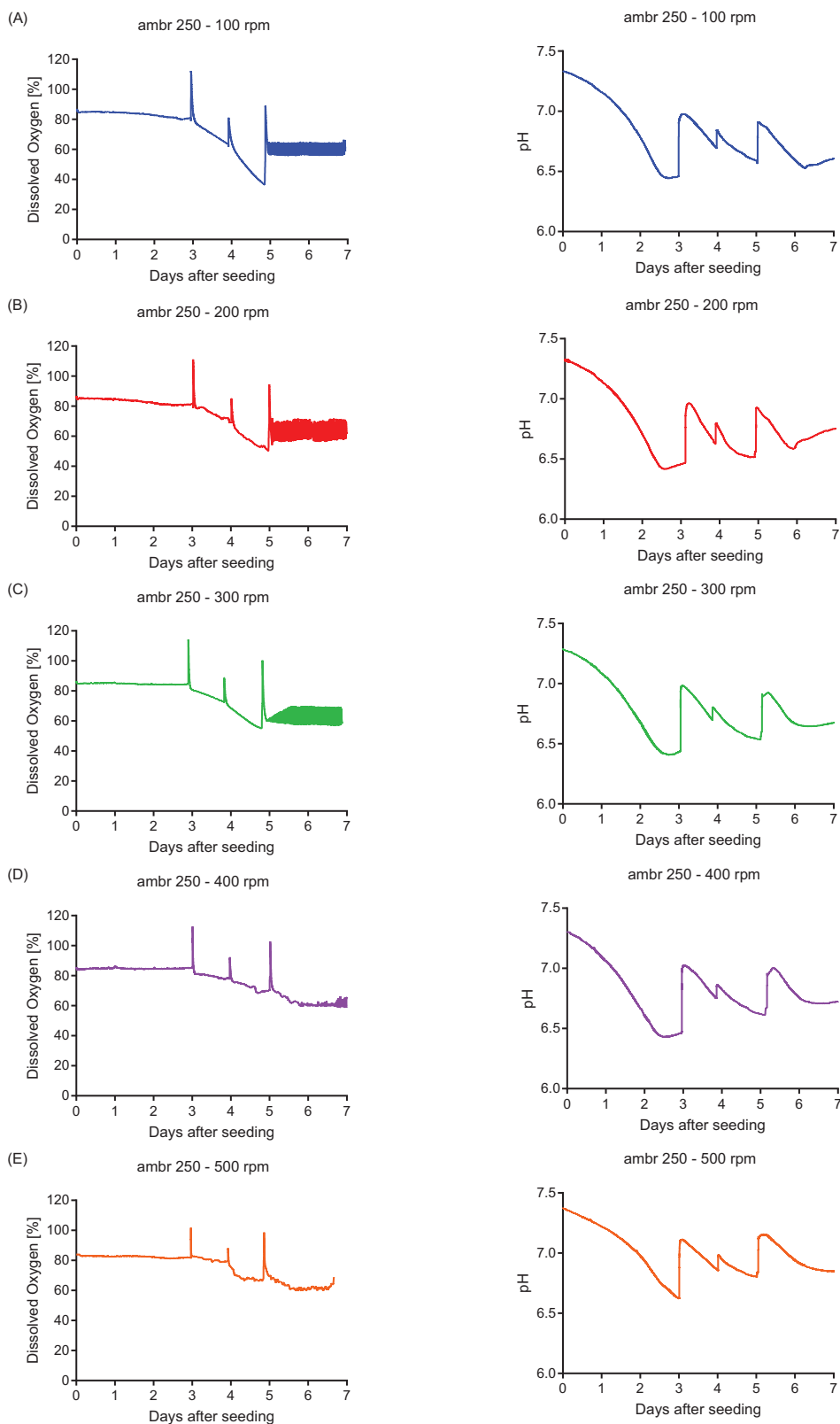


Figure 3. Representative dissolved oxygen (dO_2 ; left hand side) and pH (right hand side) trends under different agitation as the medium volume increases in the ambr 250 un baffled vessel over 7 days. In all runs, dO_2 control at 60% was introduced at day 5 after the medium exchange. A) 100 rpm, B) 200 rpm, C) 300 rpm, D) 400 rpm, and E) 500 rpm.

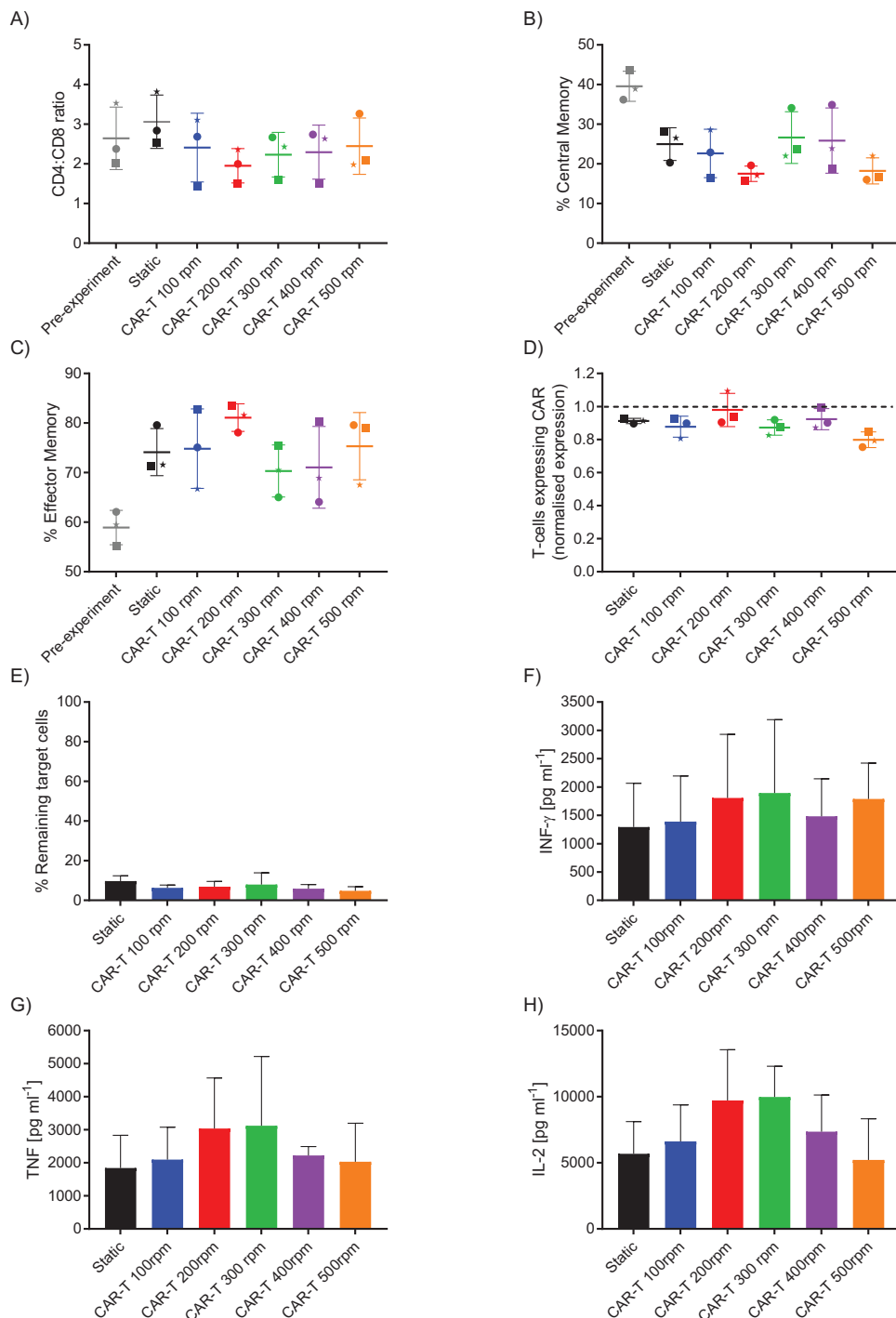


Figure 4. Phenotypic characterization of primary CAR-T cells and quantitative analysis of cytokines secreted [pg mL⁻¹] when seeded in the ambr 250 bioreactor at different speeds. Data shown mean \pm SD, $n = 3$. Each symbol represents one donor (star = HD12; circle = HD16; square = HD18). A) CD4:CD8 ratio. B) CD8+ T central memory (CCR7+ CD45RO+) subpopulation percentage of the cells. C) CD8+ T effector memory (CCR7- CD45RO+) subpopulation percentage in all the analyzed conditions. D) Normalized CAR expression at the end of the 7 days expansion. Each run has been normalized to the starting CAR expression obtained for the specific condition at inoculation (day 0). Reference line at 1 shows the equivalence in CAR expression between day 0 and day 7. Each symbol represents one donor (star = HD12; circle = HD16; square = HD18). E) Percentage of remaining target cells (NALM6) from the functionality assay. F) INF- γ concentration. G) TNF concentration. H) IL-2 concentration. No significant difference ($p > 0.05$) was found between the conditions analyzed with a one-way ANOVA test.

for each different donor and condition assessed, due to a variable transduction efficiency for each run. The percentage of T-cells expressing the CAR in all the analyzed conditions do not show any significant difference with the static control, suggesting that the fluid dynamic stresses induced by the stirring do not cause CAR shedding.

CAR-T cell functionality was assessed via an in vitro cell killing assay using NALM6 as the target cells (Figure 4E). The functionality was retained in all culture conditions where it was found to be comparable with that exhibited by the static CAR-T control with less than 10% of the target NALM6 cells remaining after 24 h across all conditions.

In addition to the immunophenotypic profile and killing assay, the culture supernatant was used to perform a CBA assay and analyze the cytokines released in the medium after coculturing CAR-T cells with CD19 expressing cells (Figure 4F–H). The CBA assay detects cytokines such as interferon-gamma (INF- γ), interleukin-2 (IL-2), and tumor necrosis factor (TNF). As shown in Figure 4F, INF- γ was released in all the conditions with no statistically significant difference between the static and dynamic conditions, as well as the TNF (Figure 4G). IL-2, an indicator of CAR-T cell proliferation, was also detected in the supernatant with again no statistically significant difference between the static and dynamic conditions (Figure 4H). The limit of the CBA assay is at 5000 pg mL⁻¹ of detected cytokine; for levels higher than that, the software extrapolates the value. We can however state that the concentration was higher than 5000 pg mL⁻¹ for all the conditions, although the plotted values might not be accurate.

3. Discussion

3.1. The Impact of Bioreactor Configuration and Agitation Intensity on CAR-T Cells Growth Kinetics

The cells used in the current work are engineered CAR-T cells expressing a second generation anti-CD19 CAR, building on the previously published study which investigated non-engineered, human primary T-cells cultured in the same unbaffled stirred tank bioreactor.^[10] As with that study, the CAR-T cells were also grown in static T-flasks as a control and we obtained similar findings; agitated conditions resulted in significantly higher cell growth kinetics with equivalent cell quality and functional profiles. This, we believe, demonstrates that T-cells (both non-transduced and genetically modified T-cells) not only retain the capacity to grow under dynamic, agitated conditions experienced in a STR, but that higher cell densities can be achieved in comparison with static conditions in a T-flask.

Of the various agitation speeds investigated, the two lowest agitation speeds employed in this study (100 and 200 rpm) were identical to those used in the previous study.^[10] However, given that the results of the previous study suggested that the 200 rpm condition resulted in improved growth compared to the 100 rpm agitation speed, in this study, we investigated even higher speeds (300, 400, and 500 rpm). We did this for two primary reasons:

First, in the earlier study, two different ambr 250 bioreactors were used, one baffled and one unbaffled with three different specific power inputs (P/M), the lowest P/M being less than that

used here at 3.1×10^{-4} W kg⁻¹. At 9.3×10^{-4} W kg⁻¹ as used here (100 rpm unbaffled), an identical P/M was used in the baffled and unbaffled bioreactors and essentially the same improved performance with human primary T-cells was attained in both configurations. The best performance was achieved at 74×10^{-4} W kg⁻¹ (200 rpm) in the unbaffled case and it was speculated that if the improvement was due to enhanced contact due to increasing turbulence between cells and Dynabeads (magnetic beads used for T-cell activation), further increases in P/M would lead to further improvement. In this study, although the agitation increases from 200 rpm up to 500 rpm (P/M from 74×10^{-4} to 1164×10^{-4} W kg⁻¹), each of these cultures performed similarly with respect to growth kinetics and cell quality, suggesting that sufficient suspension of the Dynabeads has been achieved. As in many cases involving particle suspension in stirred bioreactors, once adequate suspension is achieved, little or no further enhancement in the kinetics of a process is obtained by further increases in agitation intensity.^[11]

Second, by investigating the higher agitation speeds, it allowed us to investigate and assess the sensitivity of the CAR-T cells to hydrodynamic stresses associated with the higher agitation rates. It was found that at all the agitation conditions from 100–500 rpm (9.3×10^{-4} to 1164×10^{-4} W kg⁻¹), the viability was above 90% at harvest and the quality of the cells was as expected. Moreover, although there was little increase in growth at speeds >200 rpm (74×10^{-4} W kg⁻¹), importantly, it was noted that the cells were able to proliferate and remain >85% viable at agitation intensities up to 500 rpm (P/M as high as 1164×10^{-4} W kg⁻¹), with no adverse impact on growth potential, cell quality, or CAR-T functionality. These results clearly show that the CAR-T cells cultured in this study are not as sensitive to fluid dynamic stresses as generally believed^[12] and they can be grown quite satisfactorily in STRs. Indeed, since the faster growth led to both glucose and glutamine becoming exhausted at day 3, a different feeding strategy may well have led to higher cell densities at the higher speeds if nutrients were not a limiting factor.

To assess the likelihood of fluid dynamic stress damaging cells, the usual approach is to compare the size of the cell to that of the Kolmogorov scale of turbulence, λ_K (m):

$$\lambda_K = (\epsilon_{Tmax}/\nu^3)^{-1/4} \quad (1)$$

where ϵ_{Tmax} (W kg⁻¹) is the maximum specific energy dissipation rate close to the impeller and ν (m² s⁻¹) is the kinematic viscosity. If $\lambda_K >$ size of the cell, it should not be damaged. The precise value of the maximum to the mean specific energy dissipation rate ($=P/M$) has proved difficult to measure but based on the literature, a reasonable but high value in order to assess the likelihood of damage can be assumed.^[13] Thus, assuming that ϵ_{Tmax} is 50 times the mean specific energy dissipation rate ($=P/M$),^[14] then at 1164×10^{-4} W kg⁻¹ $\lambda_K = 16 \mu\text{m} \approx$ size of CAR-T cell. Thus, though higher speeds might lead to a deterioration in performance, the lack of damage up to this speed is not contrary to what is expected from turbulence theory.

Two other points. First, the lack of sensitivity to fluid dynamic stresses over this range suggests that if higher cell densities can be achieved by enhanced feeding strategies, higher k_1a values could be obtained in order to meet the increased oxygen demand. Second, it is not suggested that the unbaffled single impeller

bioreactor is necessarily the configuration of choice. The fact that with human primary T-cells growth was essentially the same in a baffled two impeller bioreactor at the same P/M should still be borne in mind.

3.2. Metabolites, pH, and dO_2 Kinetics during CAR-T Cell Proliferation

Once CAR-T cells are activated, they undergo extensive proliferation and significant changes in their metabolism. They switch from a catabolic metabolism to an anabolic one in order to support the proliferation and new biomass formation.^[15] Furthermore, the uptake of glucose and glutamine from the media is essential for proliferation and expression of effector functions, such as cytokine production and cytolytic molecules secretion. Both nutrients are therefore crucial for T-cell expansion and were monitored across the 7 days of culture (Figure 2).

In this work, the cells run out of glucose and glutamine on day 3 and 7 in all conditions, while glucose drops below 2 mmol L^{-1} on days 5 (before medium exchange) and 6. This drop could be a potential explanation to why, at higher speeds, the cells did not undergo better proliferation, as they run out of nutrients and therefore do not have any for further expansion. When the glucose becomes a limiting factor, the lactate production also slows down. During rapid cell proliferation, glutamine uptake results in intracellular nitrogen building up and secreted as ammonia in order to avoid toxic effects on the cells. This result explains the building up of ammonia in the medium which inversely correlates with glutamine consumption.^[15]

Glucose and glutamine consumption follow the same trend (Figure 2E,F), indicating a higher consumption per cell per day at lower speeds (100 and 200 rpm), to then reach the lower specific consumption at higher speeds (300–500 rpm). This difference is probably due to the available metabolites in these conditions. Although at 200 rpm, the final cell density is similar to the higher speeds, the available glutamine is slightly higher, justifying the higher consumption rate per cell. When there are fewer cells in the vessel (100 rpm), but the available metabolites are the same, it is logical that the uptake per cell will be higher given the greater availability of glucose/glutamine (Figure 2E,H). The same pattern can be seen in the specific lactate production, where the amount of lactate produced per cell is higher at lower speeds (Figure 2F). However, none of the conditions showed a significantly higher consumption or production of any of the metabolites. Furthermore, the lactate yield from glucose was below the theoretical limit of 2 for all the assessed speeds (Figure 2G).

It can be concluded that neither dO_2 nor pH play a significant role in this scenario, as the profiles do not show any significant differences between the different speeds (Figure 3A–E). However, at 500 rpm the dO_2 from day 5 was still slightly higher than 60% because of the higher $k_L a$ and therefore the dO_2 control was not activated; but the overall culture performance was still comparable to the other conditions. The pH profile follows a similar trend for all the speeds, starting at 7.3–7.4 and dropping to 6.4–6.5 between day 2 and 3, followed by a plateau. It has been shown that lactic acid production causes a fall in the pH profile and can impair proliferation in mammalian cell cultures if

pH reaches values lower than 6.6–6.8.^[16,17] The lower pH consequently restricts the formation of lactic acid and its accumulation in the medium. The plateau in the pH may therefore indicate the moment when the CAR-T cells run out of glucose and glutamine which combined with the low pH limits their proliferation and lactate production. The same effect can be seen in the last day of culture, when once again, the glutamine and glucose levels are down to zero. This drop to complete depletion of metabolites indicates a need to optimize the feeding strategy in order to avoid a possible rate limitation with respect to nutrient provision. Culture under such conditions would establish whether higher speeds can improve the proliferation of CAR-T cells, as it has been shown that fluid dynamic stresses do not significantly change it up to 500 rpm.

3.3. The Impact of the Fluid Dynamic Culture Environment on the Quality and Functionality of CAR-T Cells

Previous studies showed how the stirring in an ambr 250 bioreactor did not alter the phenotypic composition of the T-cell product at speeds up to 200 rpm.^[10] In this case, the speed range was extended to 500 rpm ($1164 \times 10^{-4} \text{ W kg}^{-1}$) and the cells used were transduced with an anti-CD19 CAR. T-cells markers were assessed on the day of the inoculation (pre-experiment) and at harvest (day 7) (Figure 4). There are studies suggesting that the desired CD4:CD8 ratio in the clinical products is 1:1.^[18] The ratio in the static condition was higher after the 7 day culture, while all the conditions in the bioreactor showed a lower ratio compared to the pre-experiment sample (Figure 4A). However, the lowest ratio was ≈ 2 , with no significant difference at different speeds. It has been previously reported that T-cells cultured with IL-7 and IL-15, rather than with IL-2, showed a higher proportion of CD8+ T-cells, which could help to lower the CD4:CD8 ratio toward the desired value of 1.^[19]

CD8+ T-cell subpopulation was further assessed in terms of naïve, central memory, effector memory, and terminally differentiated T-cells. The ideal CAR-T product should have a high number of naïve and central memory T-cell which increase the persistence of the drug once reinfused in the patient.^[20] The expanded cells showed a more differentiated phenotype, with less central memory cells (Figure 4B) and higher percentage of effector memory cells (Figure 4C). However, it is important to note that this was irrespective of culture platform (static T-flask or STR). These findings were expected due to the prolonged expansion protocol (14 days in total), the use of IL-2 in the medium, and a double activation of T-cells (when thawed and on day 0). The fact that there was no significant difference between the static and dynamic conditions demonstrates that fluid dynamic stresses associated with higher agitation speeds does not impact the cell immunophenotypic profile.^[10] In order to limit the differentiation of the T-cells, a shorter protocol should be put in place and the IL-2 replaced with different interleukins (IL-7, IL-15, and IL-21), which helps to maintain the undifferentiated phenotype of T-cells.^[21,22] Furthermore, cells grown with IL-7 and IL-15 (10 ng mL^{-1} each) showed a higher efficacy in vivo compared to T-cells cultured with IL-2.^[19]

The CAR expression was also assessed via flow cytometry staining on the day of the inoculation and after 7 days

expansion in both platforms (ambr 250 and T-flask). At harvest (day 7), each run was normalized to the percentage of cells expressing the CAR at inoculation (day 0), due to a variation in the initial transduction efficiency obtained for each run, ranging from 20% to 50%. At all speeds, the results were comparable to the static condition, showing that agitation over the range used here does not affect the CAR receptor shedding, expression nor CAR-T cell proliferation (Figure 4D). However, at 500 rpm the percentage of cells expressing the CAR is slightly (although not statistically significant) lower than in all other conditions. This difference might be an indication that, as hinted at by the estimate of the Kolmogorov eddy size at this speed, fluid dynamic stresses start to have an impact on the CAR receptor. Further investigations at a higher speed would be needed in order to prove this hypothesis.

The functionality assay showed comparable killing of the target cells in all the assessed conditions (static and dynamic) (Figure 4E). Engineered T-cells retained their cytolytic function even when grown at the highest agitation intensity (500 rpm, $P/M = 1164 \times 10^{-4} \text{ W kg}^{-1}$) proving that fluid dynamic stresses in this study do not affect the final product efficacy in vitro. The highest percentage of remaining NALM6 cells was found in the co-culture with CAR-T cells grown in a static condition with a mean of $9.68 \pm 2.71\%$. Efficient killing of NALM6 cells was proven in all assessed conditions, with <10% remaining NALM6 cells at 24 h. Although the normalized CAR expression was found to be lower at 500 rpm, once the CAR-T cells were isolated, they showed a low percentage of remaining target cells ($7.80 \pm 2.05\%$) showing that they retained their cytolytic function (Figure 4E).

3.4. Cytokine Secretion at Different Stirring Speeds

In order to assess the cytokines secreted by CAR-T cells, a cytometric bead array (CBA) was used to measure the concentration of different cytokines in the cell culture supernatant after co-culture with CD19 expressing cells. The cytometric bead array is used to order confirm the functionality of CAR-T cells against tumor cells in vitro, verifying the cytotoxicity data results.

A substantial secretion of proinflammatory cytokines (IL-2, TNF, and $\text{INF-}\gamma$) was detected after 24 h of co-culture with NALM6 cells (CD19 expressing cells), showing no significant difference between the assessed conditions (Figure 4F–H). Although for all three cytokines, the trend is similar, there is a higher level of cytokine for the CAR-T cells grown at 200 and 300 rpm while it drops at higher speeds. The levels of $\text{INF-}\gamma$ are in line with those found in previous work,^[19,23] when CAR-T cells are co-cultured with leukemia cells giving once again the confirmation of their functionality and cytotoxic abilities.

3.5. Comparison of the Culture of Human Primary T-Cells and Primary Human CAR-T Cells

When comparing the findings using the same agitation speeds (static T-flasks, 100 and 200 rpm) from the initial study^[10] which investigated the growth of non-engineered primary hu-

man T-cells, with the findings from this study using engineered CAR-T cells, the final cell density values were $2.38 \pm 0.25 \times 10^6$ viable cells mL^{-1} for the static T-flask control, $3.62 \pm 0.23 \times 10^6$ viable cells mL^{-1} for the 100 rpm condition, and $4.65 \pm 0.24 \times 10^6$ viable cells mL^{-1} for the 200 rpm condition. For the primary human CAR-T cells, the equivalent values were $2.56 \pm 1.38 \times 10^6$ viable cells mL^{-1} in the T-flask, $3.76 \pm 0.69 \times 10^6$ viable cells mL^{-1} at 100 rpm, and $4.99 \pm 0.77 \times 10^6$ viable cells mL^{-1} at 200 rpm. Thus, it can be concluded that the change from T-cells to CAR-T cells under identical bioreactor culture conditions has made an almost negligible impact on culture performance. This finding would therefore suggest that process development activity and growth optimization studies could be undertaken using non-engineered primary T-cells with the expectation that genetically-engineered CAR-T cells would perform similarly with respect to growth kinetics.

3.6. Manufacturing Platforms for CAR-T Cell Production

Small-scale production of CAR-T cells typically involves static cell expansion platforms, for example, T-flasks, gas-permeable bags, and G-Rex vessels. These systems are operated in batch or fed batch, require frequent manipulation (except for the G-Rex), and are difficult to scale. The gene-modified cell therapy field has recently seen the launch of closed all-in one-systems such as the Cocoon (Lonza) and the Quantum Cell Expansion System (Terumo BCT) and the CliniMACS Prodigy system (Miltenyi). However, the majority of CAR-T products manufactured for clinical trials and commercialization use a rocking motion bioreactor,^[2,24] which is a semi-closed systems that can provide better uniformity in terms of oxygenation, nutrients, and pH across the cell culture due to the mixing occurring through the rocking of the bags.^[25] A cell density at harvest of $13.2\text{--}31 \times 10^6$ cells mL^{-1} in the rocking motion platform operated under a continuous perfusion condition was reached after 13–18 days expansion.^[26] While a 16–20 fold expansion was shown in the Prodigy System after 8 days.^[27]

Here, in the best culture performance (300 rpm) in the ambr 250 STR, the final cell density reached was $\approx 5 \times 10^6$ cells mL^{-1} over a 7 day culture, which gives roughly 12.5×10^8 total live cells in a relatively small volume (250 mL). Moreover, the fold expansion at 300 rpm was 25.70 ± 1.21 , which was higher than the one reported in the CliniMACS Prodigy.^[27] If it is assumed an $\approx 40\%$ CAR-T positive population at the end of the run, this result would be 5×10^8 CAR positive viable T-cells at harvest (for a transduction efficiency as low as 20.5%, there would still be 2.56×10^8 CAR positive viable T-cells at harvest). These numbers fall in the range of target doses currently administered to patients in the FDA approved CAR-T therapies (Table 1), making a small-scale, automated STR potentially suitable for the manufacturing of personalized medicines.

Although, the cell number in the ambr 250 is significantly lower than the one reported in ref. [26], it must be noted that the rocking motion bioreactor was operated in perfusion conditions and the cells were expanded for longer (up to 18 days). Moreover, there are concerns that cells in prolonged culture may experience exhaustion and a loss of key immunophenotypic properties.^[28]

Table 1. The target dose and the maximum total number of CAR positive viable T-cells injectable in patients treated with the two FDA approved CAR-T products—YESCARTA and KYMRIAH (Data retrieved from FDA, 2019).

CAR-T product	Target dose (CAR positive viable T-cells)	Maximum total number of CAR positive viable T-cells per dose
YESCARTA	2×10^6 per kg of bodyweight	2×10^8
KYMRIAH for pediatric and young adult B-cell ALL (up to 50 kg of body weight)	$0.2\text{--}5 \times 10^6$ per kg of bodyweight	2.5×10^8
KYMRIAH for pediatric and young adult B-cell ALL (above 50 kg of body weight)	$0.1\text{--}2.5 \times 10^8$ (irrespective of body weight)	2.5×10^8
KYMRIAH for adult relapsed or refractory diffuse large B cell lymphoma	$0.6\text{--}6 \times 10^8$ (irrespective of body weight)	6×10^8

Data obtained from "Approved Cellular and Gene Therapy Products", US FDA, 2020. Copyright 2020 US Food and Drug Administration.

Results reported in ref. [27] showed a lower fold expansion in the CliniMACS Prodigy compared to those presented in this study. However, the lack of nutrients during culture seen here suggest that once the feeding strategy in the stirred bioreactor has been optimized or even switched from fed-batch to perfusion mode, it would lead to an improved performance. In particular, it should ensure that glucose and glutamine would not be a limiting factor anymore and an equivalent performance, if not better, could be achieved using STRs in comparison with rocking motion systems. Moreover, platforms such as the ambr 250, which allow for the simultaneous operation of 24 independent bioreactors enable a level of throughput and flexibility not currently seen in existing manufacturing platforms. With the move toward allogeneic CAR-T production, STRs also have proven scalability and it is not difficult to foresee multiple doses of allogeneic treatments being manufactured in >5 L stirred-tank bioreactors, with the potential for further scalability. However, further studies on the comparability between small scale and large scale bioreactors in terms of cell yields and cell functionality are needed and is an area we are actively investigating.

Although there are still open and manual process steps, transferring the process on to manufacturing technology (e.g., a bioreactor) that is far more amenable to future development toward a fully closed and automated culture step represents a large step forward on that journey and this study proves that their demonstrated performance makes it possible.

4. Conclusions

This study demonstrated, for the first time, the expansion of CAR-T cells in a STR. Building on previous work with primary T-cells, the study investigated a range of agitation intensities from 100 rpm (9.3×10^{-4} W kg⁻¹) up to 500 rpm (1164×10^{-4} W kg⁻¹) to understand the impact on CAR-T growth kinetics and quality. Agitated STR conditions resulted in higher cell densities than the static T-flask controls, with equivalent cell quality and function. It was found that an increase from 100 to 200 rpm (74×10^{-4} W kg⁻¹) led to higher cell yields ($\approx 4 \times 10^6$ cells mL⁻¹ compared to $\approx 5 \times 10^6$ cells mL⁻¹ respectively), which is in line with previous findings with primary T-cells. Similar cell densities were obtained for the 200, 300, 400, and 500 rpm agitation intensi-

ties; all speeds gave higher cell densities than the static T-flask control ($\approx 2.5 \times 10^6$ cells mL⁻¹). This finding reinforces the original hypothesis that once sufficient agitation has been achieved to ensure adequate suspension of the activating Dynabeads, the cells are able to effectively proliferate. Importantly, we demonstrated that at all agitation intensities, the quality and functionality of the CAR-T cells remained intact, retaining expression of the CAR gene and cytolytic functionality of >90% efficiency after 24 h, thereby proving that fluid dynamic stresses in this study do not affect the CAR-T cell efficacy to target and kill the leukemia cells in vitro. This study is the first demonstration of human CAR-T cell expansion in STRs with the findings presenting significant implications and opportunities for larger-scale allogeneic CAR-T production.

5. Experimental Section

Lentiviral Production: Lentiviral supernatant was produced in house using HEK 293T cell line transfected with packaging plasmids pMD2.G, pCMV-dR8.74 (Addgene plasmids #12259 and #2203), and CD19-specific CAR plasmid (gifted by Martin Pule;) using GeneJuice transfection reagent (Merck Millipore Ltd., UK). The CD19-specific CAR used in this work comprised an FMC63 scFv, a CD8 alpha stalk with a 41BB-CD3 ζ endodomain, and it was transcriptionally lined to RQR8 containing the CD34 epitope.^[29]

HEK293T cells were cultured using Dulbecco's Modified Eagle Medium (DMEM) (Gibco Thermo Fisher Scientific, Loughborough, UK) supplemented with 10% fetal bovine serum (FBS) (Thermo Fisher Scientific, Loughborough, UK) until 70% confluent. The medium was then changed to DMEM Advanced serum free medium (Gibco Thermo Fisher Scientific, Loughborough, UK) and the cells were transfected. The lentivirus was harvested 24 and 48 h post-transfection, filtered using a 0.45 μ m filter (Thermo Fisher Scientific, Loughborough, UK), and combined in a single batch. The aliquots were kept at -80 °C until use.

T-Cell Isolation, Transduction, and Pre-Expansion: Fresh peripheral blood mononuclear cells from three healthy human donors were purchased from Cambridge Bioscience (Cambridge Bioscience, UK) and T-cells were isolated as described in the previous paper.^[10] The culture medium used in this study was Roswell Park Memorial Institute (RPMI) 1640 medium (Gibco Thermo Fisher Scientific, Loughborough, UK) supplemented with 10% FBS, 2 mM L-Glutamine (Thermo Fisher Scientific, Loughborough, UK), and 30 IU mL⁻¹ interleukin-2 (IL-2; Milteny Biotech Ltd., UK). The cells were thawed in complete RPMI medium and activated using a 1:1 ratio of cell to Dynabeads (Thermo Fisher Scientific, Loughborough, UK) and seeded in a T175 Nunc non-treated flask (Thermo Fisher Scientific, Loughborough, UK) at 37 °C and 5% CO₂ in a humidified incubator.

On day 1 after thawing, the cells were transduced using lentivirus. A 6-well plate was coated overnight with 1 mL per well of a solution containing $20 \mu\text{g mL}^{-1}$ of retronectin (Takara Bio, France). After incubating the plate at 4°C overnight, the well plate was washed with phosphate saline solution and 1.5×10^6 cells were plated in each well. Each well was then topped up with 4 mL of lentiviral supernatant produced in-house and supplemented with IL-2 to achieve a final desired concentration of 100 IU. The plate was then centrifuged at 1000 g for 40 min at 32°C . Post-centrifugation, the well plate was placed into a humidified incubator at 37°C and 5% CO_2 . 24 h post-transduction, the cells were removed from retronectin, placed in a Falcon tube, and centrifuged at 300 g for 5 min. The cells were then re-suspended in complete RPMI medium and seeded into a T175 flask and pre-expanded. Complete medium was added to the cells as needed in order to maintain the cell density within the range of $1\text{--}3 \times 10^6$ cells mL^{-1} . 7 days after thawing, the cells were re-activated using 1:1 Dynabeads to cell ratio and seeded into a STR and T-flask (static control). The transduction efficiency was assessed via flow cytometry on the day of bioreactor inoculation.

ambr 250 Stirred-Tank Bioreactor Culture: An “ambr 250 high throughput” two bioreactor test system (Sartorius Stedim Biotech, UK) was used for all bioreactor studies and was equipped with single-use unbaffled vessels as described in the previous paper.^[10] The single-use unbaffled vessel had a diameter $T = 60$ mm and comprised of a single 3-segment 45° pitched blade impeller ($D = 30$ mm) with a power number, $Po = 2.1$.^[10] The specific power input, P/M (W kg^{-1}), into the medium (see Equation (2)) is

$$P/M = Po\rho N^3 D^5 / M \quad (2)$$

where P (W) is the power input, Po is the power number (dimensionless), ρ (kg m^{-3}) is the density of the medium (here assumed to have the same physical properties as water), N (rev s^{-1}) is the impeller speed, D (m) is the impeller diameter, and M is the mass of medium in the bioreactor at the end of the culture.

The impeller was operated in the down-pumping mode of operation (the direction that requires less specific power for particle suspension than up-pumping impellers^[30]), and the pH, dissolved oxygen (dO_2), temperature, and the headspace gas flow were measured continuously and monitored throughout the experiment. The ambr 250 vessels were loaded and connected to the control system and 80 mL of RPMI 1640 with 10% FBS and 2 mM L-glutamine were placed in each vessel overnight to precondition the pH probe. The seeding procedure and feeding strategy were the same as that reported in the previous study,^[10] with an initial seeding density of 0.5×10^6 cells mL^{-1} in complete RPMI medium and medium additions on day 3 (100 mL), and day 4 (50 mL). The medium exchange on day 5 was performed by removing 100 mL of cell suspension from the bioreactor and centrifuging at 350 g for 10 min, resuspended in 100 mL complete RPMI medium, and then added back to the ambr 250 vessel. The medium addition/exchange strategy in the T-flasks (static control) resembled that of the ambr 250 bioreactors. The initial impeller agitation speeds chosen for investigation were 100 and 200 rpm (9.3×10^{-4} and 74×10^{-4} W kg^{-1} , respectively), the same agitation speeds investigated in ref. [10], but as the culture demonstrated improved performance at the higher agitation speed in the original study, it was decided to investigate even higher agitation rates to see whether this trend would continue or adversely affect cell growth. As a result, agitation rates investigated included 300, 400, and 500 rpm (251×10^{-4} , 595×10^{-4} , and 1164×10^{-4} W kg^{-1} , respectively).

The headspace flow was regulated to $14.25 \text{ mL min}^{-1}$ of N_2 , with 21% O_2 and with an additional flow of CO_2 of 0.75 mL min^{-1} , as described in the previous paper.^[10] A 60% dO_2 control by gas blending with oxygen was initiated on day 5 after the medium exchange.

Analytical Techniques: A daily 1 mL sample was obtained from each vessel to measure cell density and viability with the NucleoCounter NC-3000 (ChemoMetec A/S, Denmark) using Via 1-Cassette (ChemoMetec A/S, Denmark) containing acridine orange and DAPI. The same sample was analyzed with the CuBiAn HT270 bioanalyser (Optocell GmbH & Co., KG, Germany) to obtain glucose, lactate, glutamine, and ammonia concentrations. Samples were taken before and after medium addi-

tion/exchange on days 3, 4, and 5. Once the metabolite date and viable cell number were collected, specific growth rate, doubling time, fold increase, and specific metabolite consumption rate were determined in the same way reported in the previous paper.^[10]

Immunophenotype Analysis: Phenotype analysis of the CAR-T cells was performed on the day of the inoculation in the ambr 250 vessel (7 days after thawing and 6 days after transduction) and at the end of the bioreactor culture, 7 days after inoculation. The stained samples were run on a BD LSRFortessa X-20 flow cytometer (BD Biosciences, UK) with five different lasers with excitation at 355, 405, 488, 561, and 640 nm. Two different panels of antibodies were used in this work, the first one was to assess the T-cell differentiation and included the following antibodies: CD3-BUV396, CD4-FITC, CD8-BUV737, CD197 (CCR7)-BV421, and CD45RO-PE-Cy7 (BD Biosciences, UK).

The second panel was used to assess the expression of the CAR and included the following antibodies: CD3-BUV396, CD4-FITC, CD8-BUV737, CD34-PE (Thermo Fisher Scientific, UK).^[10] A minimum of 50 000 events were recorded for each sample and the data were analyzed using FlowJo computer software (BD Biosciences, UK). Staining specificity was confirmed using fluorescence minus one controls for CCR7, CD45RO, and CD34 for each sample.

Cytotoxicity Assay: T-cells expressing the CD19-CAR were isolated using a CD34 MicroBead Kit (Milteny Biotech Ltd., UK) and LS columns (Milteny Biotech Ltd., UK) following the manufacturer’s instructions. The antibody used in the kit is an anti-CD34 antibody QBEnd10, which binds to the RQR8 protein. The cells were kept in a humidified incubator at 37°C for 24 h before being used for cytotoxicity assays. Isolated CAR-T cells were seeded at 1:1 effector:target ratio using 5×10^4 NALM6 targets per well in a 96-well plate. Non-transduced T-cells from the same donors were plated in co-culture with NALM6 at 1:1 effector:target ratio as a negative control. CAR-mediated cytotoxicity was assessed 24 h after plating via flow cytometry. T-cells were identified via CD3 (BUV395) staining and SYTOX red dead cell stain (Thermo Fisher Scientific, Loughborough, UK) was used to identify dead cells. Once the staining was performed, 25 μL of CountBright Absolute Counting Beads (Thermo Fisher Scientific, Loughborough, UK) was added to each sample in order to enable the absolute cell count. The absolute number of remaining live target cells in each condition was normalized to the negative control (non-transduced T-cells co-cultured with NALM6). The data were analyzed using FlowJo computer software.

Cytometric Bead Array Immunoassay: The same plating procedure was followed as described for the cytotoxicity assay, using isolated CAR-T cells and plating them in 96-well plates at 1:1 effector:target ratio using 5×10^4 NALM6 target cells per well. After 24 h, the plates were centrifuged at 300 g and 70 μL of supernatant were removed and placed in a new 96 conical bottom well plate (Thermo Fisher Scientific, Loughborough, UK) and placed at -80°C until the CBA immunoassay (BD Biosciences, UK) was performed as per manufacturer’s instructions. The samples were then placed into a clear round bottom 96-well plate (Corning GmbH, Germany) and run on the BS FACSVerse cytometer (BD Biosciences, UK) and data were analyzed using BD FACSuite computer software.

Statistical Analysis: Data analysis was performed using GraphPad Prism 7 software (GraphPad, La Jolla). Results are represented as mean \pm SD. A one-way analysis of variance (ANOVA) test was used and values were considered statistically significant when probability (p) values were equal or below 0.05(*), 0.01(**), 0.001(***), or 0.0001(****).

Acknowledgements

The authors would like to acknowledge Dr. Martin Pule (UCL Cancer Institute) and his team for the provision of the CAR plasmid. The authors would also like to acknowledge the funding and support of the UK Engineering and Physical Sciences Research Council (EPSRC) through the Future Targeted Healthcare Manufacturing Hub hosted at University College London with UK university partners (Grant Reference: EP/P006485/1) and includes financial and in-kind support from the consortium of industrial users and sector organizations. Funding and support from the EPSRC CDT Bioprocess Engineering Leadership (Grant Number: EP/L01520X/1)

and the EPSRC New Industrial Systems: Optimising Me Manufacturing Systems grant (Grant Number: EP/R022534/1) are also acknowledged.

Conflict of Interest

The authors declare no conflict of interest.

Keywords

bioprocessing, CAR-T cells, immunotherapy, manufacture, stirred-tank bioreactor

Received: April 15, 2020

Revised: June 1, 2020

Published online:

-
- [1] T. I. Panagopoulou, Q. A. Rafiq, *Biotechnol. Adv.* **2019**, *37*, 107411.
- [2] P. Vormittag, R. Gunn, S. Ghorashian, F. S. Veraitch, *Curr. Opin. Biotechnol.* **2018**, *53*, 164.
- [3] S. Depil, P. Duchateau, S. Grupp, G. Mufti, L. Poirot, *Nat. Rev. Drug Discovery* **2020**, *19*, 185.
- [4] Q. A. Rafiq, C. J. Hewitt, *Pharm. Bioprocess.* **2015**, *3*, 97.
- [5] A. W. Nienow, *Cytotechnology* **2006**, *50*, 9.
- [6] A. W. Nienow, B. Isailovic, T. Barrett, *Bioprocess Int.* **2016**, *14*, 12.
- [7] A. W. Nienow, K. Coopman, T. R. Heathman, Q. A. Rafiq, C. J. Hewitt, *Stem Cell Manufacturing*, Elsevier, New York **2016**, p. 43.
- [8] R. P. Harrison, S. Ruck, Q. A. Rafiq, N. Medcalf, *Biotechnol. Adv.* **2018**, *36*, 345.
- [9] Q. A. Rafiq, M. P. Hanga, T. R. Heathman, K. Coopman, A. W. Nienow, D. J. Williams, C. J. Hewitt, *Biotechnol. Bioeng.* **2017**, *114*, 2253.
- [10] E. Costariol, M. Rotondi, A. Amini, C. J. Hewitt, A. W. Nienow, T. R. Heathman, M. Micheletti, Q. A. Rafiq, *Biotechnol. Bioeng.* **2019**, *116*, 2488.
- [11] A. W. Nienow, in *Mixing in the Process Industries*, 2nd ed. (Eds: N. Harnby, M. Edwards, A. Nienow), Butterworth Heinemann, London **1997**, p. 394.
- [12] C. K. van den Bos, R. Keefe, C. Schirmaier, M. McCaman, in *Disposable Bioreactors II* (Ed: D. E. Eibl), Springer, Berlin, Heidelberg **2014**, p. 61.
- [13] A. Gabriele, A. W. Nienow, M. Simmons, *Chem. Eng. Sci.* **2009**, *64*, 126.
- [14] A. W. Nienow, C. J. Hewitt, T. R. Heathman, V. A. Glyn, G. N. Fonte, M. P. Hanga, K. Coopman, Q. A. Rafiq, *Biochem. Eng. J.* **2016**, *108*, 24.
- [15] G. J. van der Windt, E. L. Pearce, *Immunol. Rev.* **2012**, *249*, 27.
- [16] V. Konakovsky, C. Clemens, M. M. Müller, J. Bechmann, M. Berger, S. Schlatter, C. Herwig, *Bioengineering* **2016**, *3*, 5.
- [17] W. M. Miller, H. Blanch, C. Wilke, *Biotechnol. Bioeng.* **2000**, *67*, 853.
- [18] C. J. Turtle, L. A. Hanafi, C. Berger, T. A. Gooley, S. Cherian, M. Hudecek, D. Sommermeyer, K. Melville, B. Pender, T. M. Budiarto, *J. Clin. Invest.* **2016**, *126*, 2123.
- [19] E. Cha, L. Graham, M. H. Manjili, H. D. Bear, *Breast Cancer Res. Treat.* **2010**, *122*, 359.
- [20] D. Sommermeyer, M. Hudecek, P. L. Kosasih, T. Gogishvili, D. G. Maloney, C. J. Turtle, S. R. Riddell, *Leukemia* **2016**, *30*, 492.
- [21] N. Singh, J. Perazzelli, S. A. Grupp, D. M. Barrett, *Sci. Transl. Med.* **2016**, *8*, 320ra3.
- [22] M. Sabatino, J. Hu, M. Sommariva, S. Gautam, V. Fellowes, J. D. Hocker, S. Dougherty, H. Qin, C. A. Klebanoff, T. J. Fry, *Blood* **2016**, *128*, 519.
- [23] J. N. Kochenderfer, M. E. Dudley, S. A. Feldman, W. H. Wilson, D. E. Spaner, I. Maric, M. Stetler-Stevenson, G. Q. Phan, M. S. Hughes, R. M. Sherry, J. C. Yang, U. S. Kammula, L. Devillier, R. Carpenter, D. A. Nathan, R. A. Morgan, C. Laurencot, S. A. Rosenberg, *Blood* **2012**, *119*, 2709.
- [24] X. Wang, I. Rivière, *Cancer Gene Ther.* **2015**, *22*, 85.
- [25] R. P. Somerville, L. Devillier, M. R. Parkhurst, S. A. Rosenberg, M. E. Dudley, *J. Transl. Med.* **2012**, *10*, 69.
- [26] D. Hollyman, J. Stefanski, M. Przybylowski, S. Bartido, O. Borquez-Ojeda, C. Taylor, R. Yeh, V. Capacio, M. Olszewska, J. Hosey, *J. Immunother.* **2009**, *32*, 169.
- [27] W. Zhang, K. R. Jordan, B. Schulte, E. Purev, *Drug Des., Dev. Ther.* **2018**, *12*, 3343.
- [28] S. Ghassemi, S. Nunez-Cruz, R. S. O'Connor, J. A. Fraietta, P. R. Patel, J. Scholler, D. M. Barrett, S. M. Lundh, M. M. Davis, F. Bedoya, *Cancer Immunol. Res.* **2018**, *6*, 1100.
- [29] B. Philip, E. Kokalaki, L. Mekkaoui, S. Thomas, K. Straathof, B. Flutter, V. Marin, T. Marafioti, R. Chakraverty, D. Linch, *Blood* **2014**, *124*, 1277.
- [30] A. W. Nienow, in *Mixing in the Process Industries*, 2nd ed. (Eds: N. Harnby, M. Edwards, A. Nienow), Butterworth Heinemann, London **1997**, p. 364.